

## 2D reconstruction of magnetotail electron diffusion region measured by MMS

J. M. Schroeder<sup>1</sup>, J. Egedal<sup>1</sup>, G. Cozzani<sup>2</sup>, Yu. V. Khotyaintsev<sup>3</sup>,  
W. Daughton<sup>4</sup>, R. E. Denton<sup>5</sup>, J. L. Burch<sup>6</sup>

<sup>1</sup>Department of Physics, University of Wisconsin-Madison, Madison, Wisconsin 53706, USA

<sup>2</sup>Department of Physics, University of Helsinki, Helsinki, Finland

<sup>3</sup>Swedish Institute of Space Physics, Uppsala 75121, Sweden

<sup>4</sup>Los Alamos National Laboratory, Los Alamos, New Mexico 87545, USA

<sup>5</sup>Department of Physics and Astronomy, Dartmouth College, Hanover, NH, USA

<sup>6</sup>Southwest Research Institute, San Antonio, TX, USA

### Key Points:

- The fluctuating measurements are consistent with a 2D reconnecting geometry, permitting a detailed spacecraft trajectory to be determined.
- The MMS data is projected onto a 2D spatial domain, revealing the fine-scale structure of the electron diffusion region (EDR).
- The EDR includes profiles with strong gradients in fields and flows, consistent with those observed in a matched 2D kinetic simulation.

arXiv:2209.11935v1 [physics.space-ph] 24 Sep 2022

## Abstract

Models for collisionless magnetic reconnection in near-Earth space are distinctly characterized as 2D or 3D. In 2D kinetic models, the frozen-in law for the electron fluid is usually broken by laminar dynamics involving structures set by the electron orbit size, while in 3D models the width of the electron diffusion region is broadened by turbulent effects. We present an analysis of *in situ* spacecraft observations from the Earth's magnetotail of a fortuitous encounter with an active reconnection region, mapping the observations onto a 2D spatial domain. While the event likely was perturbed by low-frequency 3D dynamics, the structure of the electron diffusion region remains consistent with results from a 2D kinetic simulation. As such, the event represents a unique validation of 2D kinetic, and laminar reconnection models.

## Plain Language Summary

Magnetic reconnection is a fundamental process that occurs in the near-Earth space environment with implications for the safety and longevity of space-borne electronics in which magnetic field lines rearrange and release energy. To understand whether reconnection is better described as occurring in a 2D-plane without variation in the third direction versus 3D with variation in all directions, we analyze spacecraft data from the night-side of Earth's magnetic field. We conclude for the considered event that the innermost region, where the field lines reconnect, remains consistent with results from a 2D simulation.

## 1 Introduction

Magnetic reconnection (Dungey, 1953) is a fundamental physical process in plasmas in which magnetic field lines rearrange their topology and convert magnetic energy into particle thermal and kinetic energies (Zweibel & Yamada, 2009). Despite a large body of research on this topic, the precise physics of what occurs at the smallest scales in these reconnection events is yet to be fully understood. One outstanding question is whether structures of the innermost reconnection region where the electron fluid decouples from the magnetic field, called the electron diffusion region (EDR), are best described by laminar, 2D kinetic models (Vasyliunas, 1975; Pritchett, 2001) or by 3D models that predict instabilities that broaden features of the reconnection site (Papadopoulos, 1977; Huba et al., 1977; Hoshino, 1991). To address this issue, NASA recently launched the Magnetospheric Multiscale Mission (MMS), which orbits about Earth's magnetosphere and is designed specifically to probe the small-scale structure of magnetic reconnection *in situ* (Burch et al., 2016). We here revisit one out of several electron diffusion regions observed by MMS in the Earth's magnetotail, with the aim to compare the recorded dynamics to numerical results obtained with a 2D kinetic simulation model.

## 2 Summary of MMS event

On August 10, 2017 MMS observed a reconnection event in Earth's magnetotail. During this event the spacecraft flew fortuitously along a topological boundary between plasma inflow and outflow, also known as a magnetic separatrix, and straight through the center of a reconnection EDR. The event has been the subject of previous investigations (Zhou et al., 2019; Hasegawa et al., 2022; Denton et al., 2020; Cozzani et al., 2021). In Cozzani et al. (2021), the frequency of strong fluctuations in fields and flows are found to be consistent with kinking of the current sheet in the direction normal to the reconnection plane at the lower-hybrid frequency. In addition, the signals could also be influenced by the reconnection exhaust separatrices being rippled by small magnetic islands (Denton et al., 2020). While 3D geometry and time-dependent dynamics are sug-

gested to describe the observation, whether the nature of the event can be accounted for by a 2D laminar framework is still not fully determined. Considering the same event, we here explore in greater detail the evidence for 2D or 3D reconnection dynamics. We seek to address the extent to which the observed signals are consistent with a 2D reconnection geometry that is being “pushed around” as a rigid body by Alfvénic perturbations external to the EDR. The stronger fluctuations observed in the vicinity of the EDR could then be interpreted as the result of the spacecraft zigzagging through the reference frame of a static 2D geometry with strong spatial gradients, rather than caused by a localized 3D instability.

In Fig. 1(a-e) several key measurements by MMS are shown in the time interval of the reconnection encounter. The observation of a reversal in the  $B_L$  magnetic field component (seen near 12:18:33 UTC in panel a) bracketed by strong electron temperature anisotropy (panel b) indicate an EDR encounter where the MMS path sampled the EDR as well as the boundaries of the two opposing inflow regions, since reconnection inflows are typically characterized by enhanced parallel electron temperature. Additionally, the normal electric field and electron outflow velocity profiles include significant fluctuations shortly after the  $B_L$  reversal. The times within the grey dashed bars in panels a-e indicate the region of interest and are chosen to encompass the features described above. We will call this interval the reconnection region, as MMS samples both the EDR and along the magnetic separatrix. The reconstructed signals in Fig. 1(f-j) will be discussed in further detail at the end of the manuscript, but to the extent that they agree with the corresponding signals in Fig. 1(a-e), they show that a 2D reconnection geometry is consistent with the observation.

To examine the characteristics of the fluctuations present in the EDR, in Fig. 2(a) the high-pass filtered  $B_L$  signal is shown for a wider time interval, where  $\Delta t=0$  corresponds to 12:18:30 UTC. The  $B_L$  fluctuations, denoted  $\delta B_L$ , exhibit a notable increase in amplitude in the reconnection region. We first seek to characterize the gradient length scale typical for various quantities across the reconnection encounter. In turn, this will allow us to compute the level of displacement  $\delta \mathbf{x}$  required by a hypothetical 2D rigid geometry to account for the observed fluctuation levels.

In Fig. 2(a) the orange curve represents the magnitude of the spatial gradient in  $B_L$  calculated to linear order using low-pass filtered data (Paschmann & Daly, 1998). Normalizing the fluctuations by this gradient scale yields a quantity denoted as  $\delta \mathbf{x} = \delta B_L / |\nabla B_L|$  in Fig. 2(b), which represents the plasma excursion projected along  $\nabla B_L$ . Significant to the present analysis, we observe that this displacement measure,  $\delta \mathbf{x}$ , has approximately constant amplitude inside and outside of the reconnection region. To further address if the displacement amplitude is uniform or peaked at the reconnection region, we examine the amplitude Fourier spectrum for the fluctuations in Figs. 2(a,b) at different time intervals. In panel (c) we show  $\langle A_{\delta B_L} \rangle_{\text{MMS}}$ , the mean amplitude of the  $B_L$  fluctuations for all four spacecraft, over three 10 second time intervals. The first of these, beginning at  $\Delta t = 0$ s, covers the crossing of the x-line and the most significant fluctuation amplitude in  $B_L$  (between the grey dashed lines in panels (a,b), approximately matching the grey reconnection interval in Fig. 1). The two other time intervals are chosen to start at  $\Delta t = 25$ s and  $\Delta t = 45$ s, which we estimate to be about  $5d_i$  and  $9d_i$  from the x-line, respectively, based on extrapolating the velocity of the spacecraft trajectory discussed in the next section ( $d_i = c/\omega_{pi}$  is the ion inertial length). In panel (d) we compute  $\langle A_{\delta \mathbf{x}} \rangle_{\text{MMS}}$  over the same time intervals. All spectra exhibit a noisy profile of spectral amplitude peaking around 1-2 Hz. While the  $B_L$  fluctuations have considerably stronger power during the central current sheet crossing, the excursion  $\delta \mathbf{x}$  appears larger outside the EDR. It should be noted that the second time interval occurs at times with significant  $B_N$  variation and the third over a quieter period. Time intervals over different field structures display different spectral features from those chosen here, but importantly the  $\delta \mathbf{x}$  fluctuation amplitude at the current sheet crossing does not dom-

inate over other intervals in the same way as  $\delta B_L$ . We additionally repeated this analysis with other components of the magnetic field and found that gradients in those quantities are much smaller and lead to unrealistically high values of  $\delta \mathbf{x}$ ; however, other quantities such as fluctuations in electron flow speed yield similar results.

The observations based on Fig. 2 provide evidence that the fluctuations observed within the EDR are influenced by large-scale fluctuations of the magnetotail current sheet not generated by the reconnection event itself. From Fig. 2(d), using the peak frequency  $f \simeq 1.5\text{Hz}$  and the mean amplitude  $\langle A_{\delta \mathbf{x}} \rangle_{\text{MMS}} \simeq 2.75\text{km/Hz}$ , we estimate a typical perturbation speed as  $v_{fluct} = 2\pi f \langle A_{\delta \mathbf{x}} \rangle_{\text{MMS}} \simeq 25\text{km/s}$ . This speed is small compared to the upstream Alfvén speed,  $V_{A\infty} \simeq 400\text{km/s}$ , providing additional evidence that the fluctuations observed within the EDR are imposed by modest Alfvénic perturbations existing throughout the reconnecting current sheet. These perturbations likely include kinking of the current sheet at scales larger than the 2D plane as discussed in Cozzani et al. (2021) and possibly other types of Alfvénic waves. The present small level of activity is also in contrast to the event in Li et al. (2021), in which fluctuations of  $\delta \mathbf{E}$  near the EDR were elevated by orders of magnitudes above the background level of upper hybrid waves. In addition to externally imposed fluctuations, below we find that features in the  $B_N$  measurement indicate that magnetic islands as identified in Denton et al. (2020) may also be a source for ripples in the separator.

### 3 Comparison to kinetic simulation

We now explore the extent to which the observed signals are compatible with results from a 2D kinetic simulation. We apply VPIC particle-in-cell code (Bowers et al., 2009), which is used extensively to study magnetic reconnection. As in Cozzani et al. (2021), the numerical run initialized with a normalized upstream plasma beta  $\beta_{e,\infty} = 0.09$ , temperature ratios  $T_{i,\infty}/T_{e,\infty} = 5$ , and a guide-field  $B_g/B_0 = 0.1$ . However, compared to Cozzani et al. (2021) we use an earlier time slice, which has a 30% lower reconnection rate and reduced separator angles yielding better agreement with the observations. The simulation uses the full proton to electron mass ratio,  $m_i/m_e = 1836$ , which allows for a direct quantitative mapping between VPIC and MMS units (Egedal et al., 2019). As discussed in Le et al. (2013), the guide magnetic field  $0.05 < B_g/B_0 < 0.15$  renders this a Regime II event with no extended electron jets expected to emanate beyond a localized EDR.

In Fig. 3 the inferred spacecraft paths are plotted over VPIC data for the electron temperature anisotropy, characterized by the ratio of electron temperature parallel and perpendicular to magnetic field lines. The paths are found through a least-squares optimization procedure, similar to that laid out in Egedal et al. (2019). However, for the present analysis, the MMS1  $B_L$  signal directly determines the simulation  $B_L$  contour along which the spacecraft position is optimized. Further details of this procedure are discussed in Section 1 of the Supporting Information accompanying this text.

With the paths of the spacecraft determined, the raw time series data from all four can be spatially binned and averaged to construct 2D maps of the event in the  $LN$ -plane. Technical details of this procedure are laid out in Section 2 of the Supporting Information document. The result is shown in the leftmost column of Fig. 4, where MMS reconstructions for twelve different spacecraft measurement fields are shown. The corresponding VPIC simulation data are shown in the middle and right columns. The middle and right columns contain the same VPIC data values, but the middle column is restricted to the same domain as the MMS data for better visual comparison. The cyan contour of Fig. 3 becomes the nearly horizontal black line in the reconstructed maps. The other simulation separatrix, not shown in Fig. 3, is included to highlight inflow and outflow regions distinctly. These contours represent the exact simulation separatrices and are laid over the MMS panels for reference, not to indicate the physical separatrices for the ob-

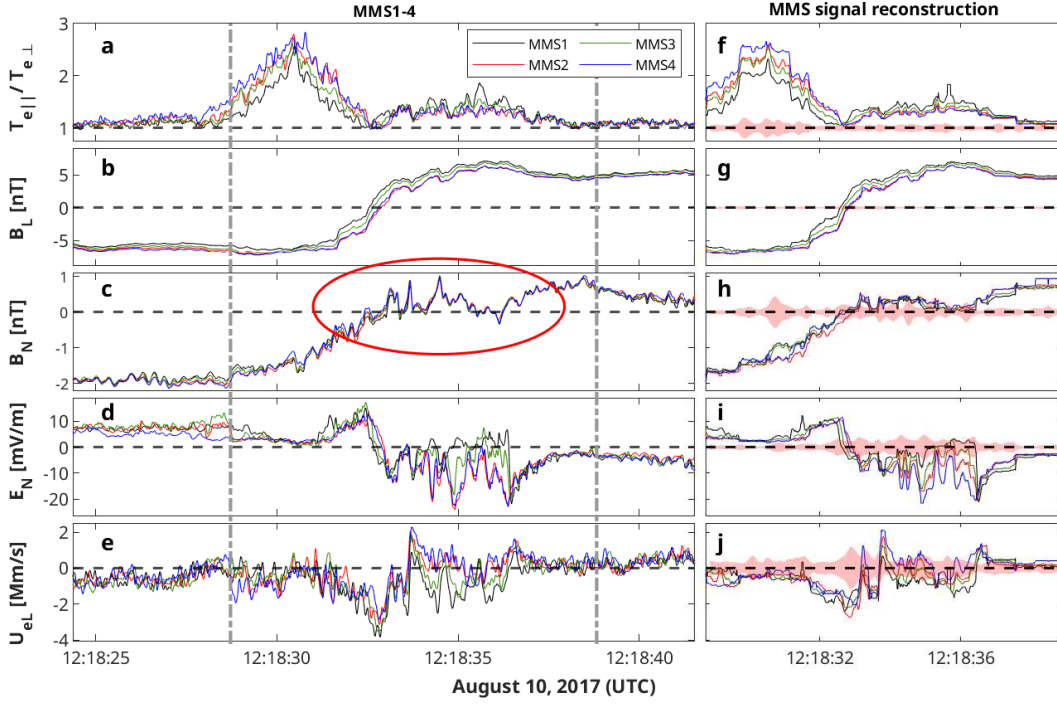


**Figure 1.** Time series data from the magnetotail reconnection event measured on August 10, 2017. Shown from top to bottom are (a) temperature anisotropy, (b/c) magnetic field in the  $L/N$ -direction, (d) electric field in the  $N$ -direction, and (e) electron velocity in the  $L$ -direction. We use the previously determined event basis of Denton et al. (2020), where unit vectors in geocentric solar ecliptic (GSE) coordinates are  $[\mathbf{L};\mathbf{M};\mathbf{N}] = [0.9872, -0.1305, -0.0915; 0.1580, 0.8782, 0.4515; 0.0214, -0.4601, 0.8876]$ , aligning the separatrix in the MMS event with the corresponding separatrix in the VPIC simulation. (f-j) show the result of interpolation through 2D maps of Fig. 4 along the spacecraft paths shown in Fig. 3. Shaded in pink in is the reconstruction error, taken as the root-mean-square of the differences between the measured signal and the reconstructed signal for MMS1-4.

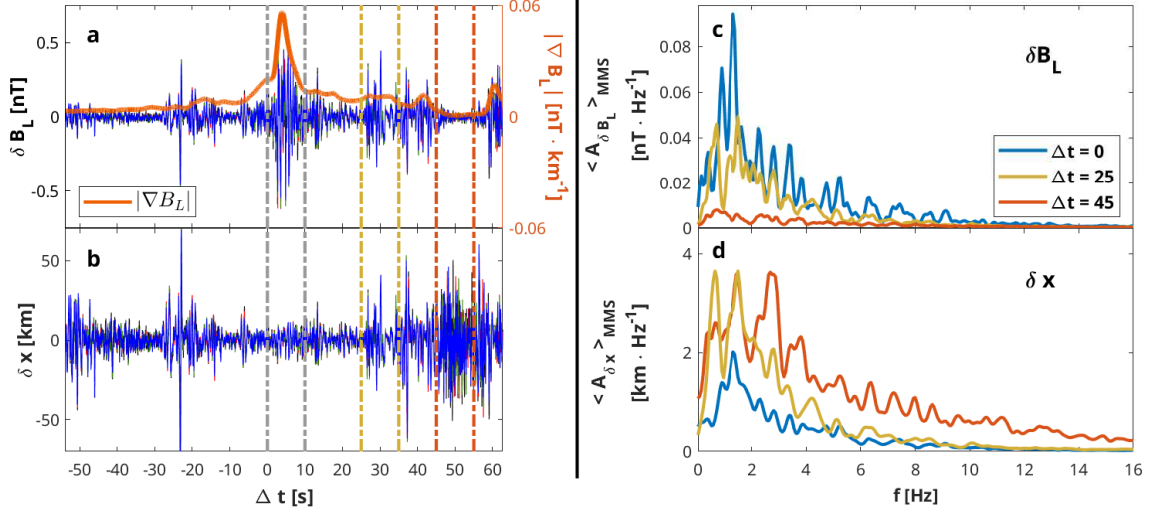


**Figure 2.** (a) Fluctuations in the magnetic field in the  $L$ -direction,  $\delta B_L$ , for each spacecraft are shown. A peak in fluctuations can be seen near  $\Delta t=5$ . We compute the high-pass filtered signal by subtracting the Gaussian-smoothed mean signal from the measurement, using a Gaussian with a width of 1s. (b) The plasma excursion,  $\delta x = \delta B_L/|\nabla B_L|$ . (c) Amplitude spectra of fluctuations in  $B_L$  over 10 second time intervals averaged across all four spacecraft,  $\langle A_{\delta B_L} \rangle_{\text{MMS}}$ . Shown are three spectra, one starting at the current sheet crossing  $\Delta t=0$ s and the other two at later times of  $\Delta t=25$ s and  $\Delta t=45$ s. (d)  $\langle A_{\delta x} \rangle_{\text{MMS}}$  for the same three time intervals considered in (c).

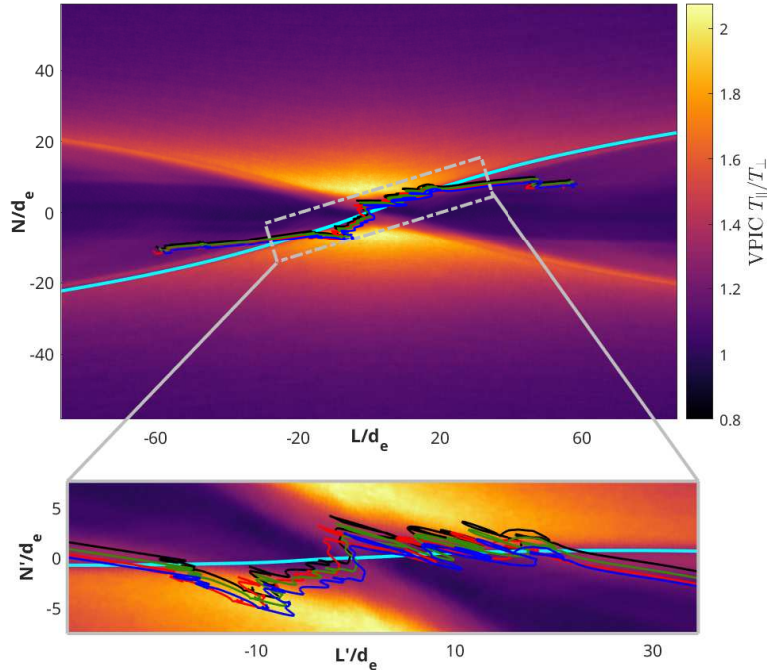


**Figure 3.** Upper panel: The spacecraft paths are plotted over VPIC simulation data of the ratio of electron temperatures parallel and perpendicular to the magnetic field. One of the two magnetic separatrices, plotted as a cyan curve, is used as the basis of a coordinate transform in 2D MMS plots shown in Fig. 4. Lower panel: Zoomed in view of the domain and coordinates used for 2D reconstruction.

served event. Lastly, the spacecraft paths in the rotated coordinates are superimposed on the first VPIC panel in the second column.

Visual comparison of the reconstructed maps to the simulation data shows striking similarity in many key features in each quantity. Sharp gradients across the separator around  $L'/d_e \sim 10\text{-}25$  are seen in multiple fields including  $E_N$  where a variation along  $N'$  of  $\sim 25\text{mV/m}$  over  $\sim 2d_e$  matches excellently with the simulation data. As described above, at each time-point, the optimization for the four spacecraft locations only includes a single degree of freedom. Therefore, the good match between multiple MMS maps and VPIC profiles is direct evidence that the EDR has a rigid 2D structure, without strong 3D effects or fast temporal variations. For example, had the event included significant 3D dynamics that broaden separatrix layers, sharp gradients in multiple quantities (including the elements of  $\mathbf{E}$  and  $\mathbf{u}_e$ ) would be smoothed out by the overlapping  $LN$ -projected spacecraft paths. Good quantitative agreement is also observed between the MMS and VPIC quantities, but to fit a common color map, the VPIC profiles of  $n_e$ ,  $T_{e\perp}$ ,  $P_{eLM}$ , and  $P_{eMN}$  in Fig. 4 are each multiplied by a factor of 1.3. This suggests that the value of  $\beta_{e\infty}$  applied in the simulation could still be optimized further. However, this simulation parameter is not expected to influence the accuracy of the presented 2D MMS data profiles.

To further illustrate how the 2D reconstructed maps well represent the observation, we construct time series data directly comparable to the MMS signals by interpolating the 2D maps along each respective spacecraft path. This is presented in Fig. 1(f-j), where the measured MMS signals of four key fields are in the left column while the interpolated signals are shown in the right column. Good agreement is seen for each field, confirming the accuracy of the reconstructed 2D maps of the event. The pink shaded regions in the second column are error estimates for the reconstruction, the root-mean-square of the difference between MMS measurement and the reconstructed signal across all four spacecraft. The error estimate for  $B_L$  is particularly small because that quantity is fixed to the MMS1 measurement in the trajectory optimization (see Supporting Information, Section 1). In other fields, however, the error remains bounded to a small value for all times and thus indicates the merit of the 2D reconstruction method.

Having shown that a 2D geometry well suits the event considered, we now consider the in-plane magnetic field profile and separatrix locations for the spacecraft observation. The in-plane magnetic field fulfills  $\mathbf{B}_{LN} = \nabla \times A_M \mathbf{e}_M$ , where  $A_M$  is the  $M$ -component of the magnetic vector potential, so it follows that  $A_M(L, N) = \int_{L_0, N_0}^{L, N} \mathbf{B}_{LN} \times \vec{d\ell}_{LN}$  (Kesich et al., 2008). Here the integral can be carried out along an arbitrary path from an arbitrary starting point  $(L_0, N_0)$ . In Fig. 4 the MMS profiles of  $B_L$  and  $B_N$  are relatively smooth and we can interpolate where possible in the  $L'$  direction to obtain an enhanced area of coverage.  $A_M(L, N)$  is then obtained by first integrating from  $L'/d_e = -30$  to  $L'/d_e = 30$  along the center of the domain where  $\mathbf{B}_{LN}$  data is available, characterizing  $A_M(L', N')$  along this center-line. Any point in the  $(L', N')$ -plane is then reached by integrating in  $N'$ -direction from the center-line.

The result is shown in Fig. 5, where black lines represent contours of constant  $A_M$  and the red lines represent the topological separatrices. To the best of our knowledge, this is the first map of the field lines in a region of an EDR obtained directly by MMS data without relying on any extrapolation techniques. The present magnetic map is based on all the data of the EDR encounter and covers a spatial domain of about  $60d_e$  along the separatrix.

We observe how the separatrices mark the locations of the strongest gradients in  $E_N$ ,  $U_{eL}$  and  $U_{eM}$ , where the gradient length scale for these quantities is at or below  $1d_e$ . Such fine-scale structures are not expected in scenarios including strong instabilities and/or 3D dynamics, which have been shown to broaden reconnection current layers by provid-

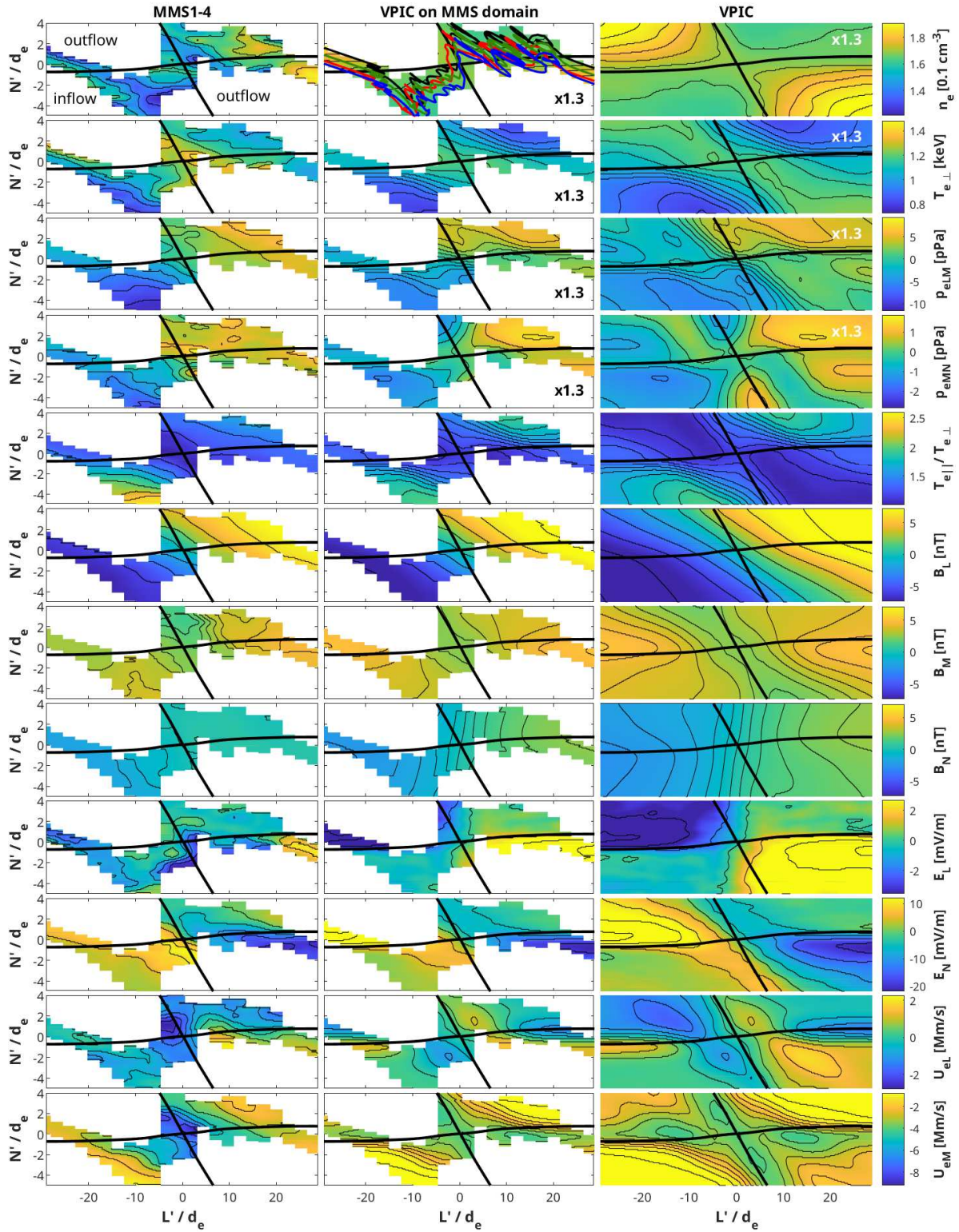


**Figure 4.** The left column shows fields measured with MMS constructed into a 2D map based on the spacecraft trajectory. The map is given in rotated coordinates  $(L', N')/d_e$ , where  $L'$  approximately represents the distance along and  $N'$  the distance away from the separatrix highlighted in cyan in Fig. 3 (shown here as a horizontal black curve). The middle column shows VPIC data of the same region of the reconnection geometry for comparison, and the right column shows VPIC data over the entire domain plotted. The top panel of the VPIC data in the middle column is overlaid with the spacecraft paths in the rotated coordinates. The first four fields of VPIC data are multiplied by a factor of 1.3 for better visual comparison to the MMS data.



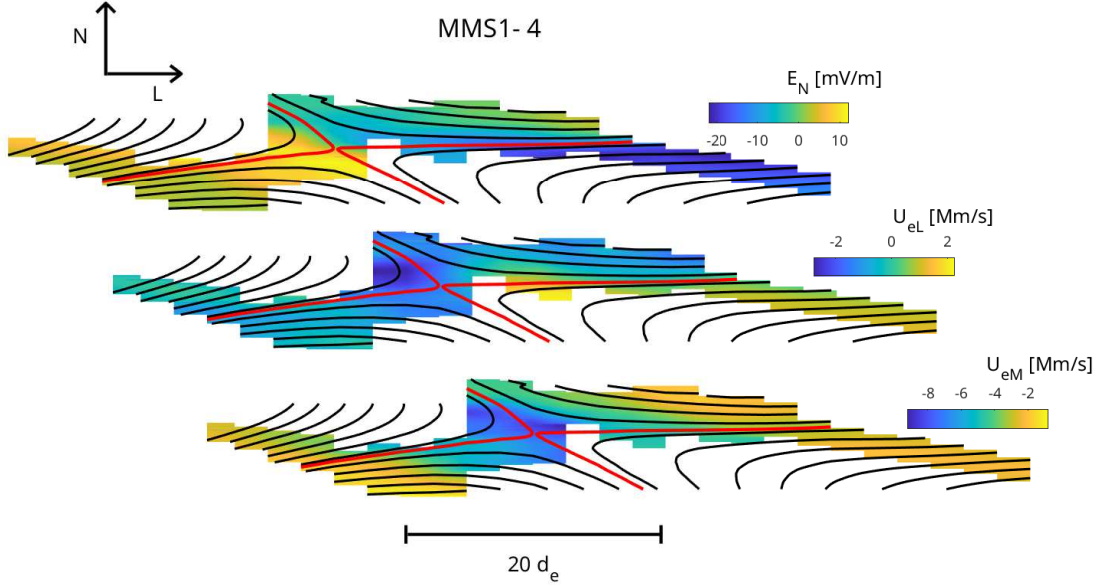


**Figure 5.** MMS maps from Fig. 4 in  $L'N'$ -coordinates. Overlaid are magnetic field lines in the  $LN$ -plane calculated from  $A_M$  contours, where  $A_M$  is obtained directly from MMS 2D maps of  $B_L$  and  $B_N$ . Contours that fall outside of underlying color plot come from interpolation of magnetic field maps along the  $L'$ -direction.

ing an additional source of electron diffusion (Graham et al., 2022). Their presence thus provides additional validation of the 2D structure assumed in the the analysis.

However, the spatial resolution is limited by the bin-size ( $\simeq 2d_e$ ) applied in the  $L'$ -direction, and this resolution does not allow us to identify magnetic islands at this scale. This can also be seen in Fig. 1(c/h), where the MMS measurements of  $B_N$  display oscillations including sign reversals around times 12:18:32-12:18:37 (circled in red). These oscillations in the  $N$ -direction are likely due to island structures previously reported (Hasegawa et al., 2022; Denton et al., 2020). Meanwhile, the  $B_N$  oscillations are not as prominent in the reconstructed signals averaged out by the finite resolution of our analysis. The oscillations not captured in the reconstruction are observed to have a magnitude of about  $\Delta B_N \simeq 0.5$  nT, which should be compared to  $B_L \simeq 5$  nT. In the  $L'$ -direction the “wave-length” of fluctuations about the separatrix is about  $\lambda \simeq 5d_e$ , such that the  $B_N$  fluctuations correspond to a  $(0.5/5)5d_e = 0.5d_e$  ripple in the separatrix, not captured by the reconstruction. Thus, this effect alone is unlikely to account for the inferred magnitude of oscillations ( $\simeq 4d_e$ ) in the spacecraft trajectories.

## 4 Conclusions

In summary, we apply particle-in-cell simulation to analyze the Aug. 10, 2017 EDR event. Direct quantitative comparison provides optimized spacecraft trajectories that give spatial information in the 2D reconnection plane. Reconstruction of measured quantities in this plane provide a unique and detailed picture of the electron diffusion region with sub-electron scale resolution. The 2D reconstructions fit the underlying simulation with good accuracy suggesting that the present event has an inherently 2D-nature in agreement with results from 2D kinetic simulations. Our results are also consistent with results of Zhou et al. (2019), which conclude the event is mostly laminar with weak wave activity. The fluctuations in signals observed are well accounted for by the short gradient length-scale ( $< 1d_e$ ) of the EDR, which we characterize as a rigid body being jostled by a bath of large-scale, low-amplitude fluctuations. The spatial displacements as-

sociated with these fluctuations are consistent with Alfvénic fluctuations observed external to the EDR, and while magnetic islands likely are present within the EDR, the data suggest that external fluctuations are responsible for the oscillatory motion of the spacecraft through the rigid 2D reconnection geometry. The reconstructed flux-function as well as the agreement of the 2D reconnection structure with those of the simulation provide a unique confirmation of laminar 2D kinetic models for reconnection.

### Acknowledgments

The work was funded by an H. I. Romnes Faculty Fellowship by the UW-Madison Office of the Vice Chancellor for Research and Graduate Education.

### Open Research

The Magnetospheric Multiscale Mission (MMS) data used in this paper is publicly available from the CU-Boulder Laboratory for Atmospheric and Space Physics MMS Data Center webpage (<https://lasp.colorado.edu/mms/sdc/public/>). Using the initial conditions specified in the text, the numerical data can be reproduced with the open source VPIC code available at <https://github.com/lanl/vpic>, as well as at <https://zenodo.org/record/4041845#.X2kA1x17kuY> (doi - 10.5281/zenodo.4041845).

### References

- Bowers, K., Albright, B., Yin, L., Daughton, W., Roytershteyn, V., Bergen, B., & Kwan, T. (2009, 2009). Advances in petascale kinetic plasma simulation with VPIC and Roadrunner [Journal Paper]. *Journal of Physics: Conference Series*, *180*, 012055 (10 pp.).
- Burch, J. L., Moore, T. E., Torbert, R. B., & Giles, B. L. (2016, MAR). Magnetospheric Multiscale Overview and Science Objectives. *Space Science Reviews*, *199*(1-4), 5-21. doi: {10.1007/s11214-015-0164-9}
- Cozzani, G., Khotyaintsev, Y. V., Graham, D. B., Egedal, J., André, M., Vaivads, A., ... Burch, J. L. (2021, Nov). Structure of a perturbed magnetic reconnection electron diffusion region in the earth's magnetotail. *Phys. Rev. Lett.*, *127*, 215101. Retrieved from <https://link.aps.org/doi/10.1103/PhysRevLett.127.215101> doi: 10.1103/PhysRevLett.127.215101
- Denton, R. E., Torbert, R. B., Hasegawa, H., Dors, I., Genestreti, K. J., Argall, M. R., ... Fischer, D. (2020). Polynomial reconstruction of the reconnection magnetic field observed by multiple spacecraft. *Journal of Geophysical Research: Space Physics*, *125*(2), e2019JA027481. doi: <https://doi.org/10.1029/2019JA027481>
- Dungey, J. (1953). Conditions for the occurrence of electrical discharges in astrophysical systems. *Philosophical Magazine*, *44*, 725.
- Egedal, J., Ng, J., Le, A., Daughton, W., Wetherton, B., Dorelli, J., ... Rager, A. (2019, Nov). Pressure tensor elements breaking the frozen-in law during reconnection in earth's magnetotail. *Phys. Rev. Lett.*, *123*, 225101. Retrieved from <https://link.aps.org/doi/10.1103/PhysRevLett.123.225101> doi: 10.1103/PhysRevLett.123.225101
- Graham, D., Khotyaintsev, Y., André, M., Vaivads, A., Divin, A., Drake, J., ... Dokgo, K. (2022, May). Direct observations of anomalous resistivity and diffusion in collisionless plasma. *Nature Communications*, *13*(1), 2954. Retrieved from <https://hal.archives-ouvertes.fr/hal-03697620> doi: 10.1038/s41467-022-30561-8
- Hasegawa, H., Denton, R. E., Nakamura, T. K. M., Genestreti, K. J., Phan, T. D., Nakamura, R., ... Saito, Y. (2022). Magnetic field annihilation in a magnetotail electron diffusion region with electron-scale magnetic islands. *Journal of*

- Geophysical Research: Space Physics*, 127.
- Hoshino, M. (1991). Forced magnetic reconnection in a plasma sheet with localized resistivity profile excited by lower hybrid drift type instability. *Journal of Geophysical Research: Space Physics*, 96(A7), 11555-11567. Retrieved from <https://agupubs.onlinelibrary.wiley.com/doi/abs/10.1029/91JA00984> doi: 10.1029/91JA00984
- Huba, J. D., Gladd, N. T., & Papadopoulos, K. (1977). The lower-hybrid-drift instability as a source of anomalous resistivity for magnetic field line reconnection. *Geophysical Research Letters*, 4(3), 125-128. Retrieved from <https://agupubs.onlinelibrary.wiley.com/doi/abs/10.1029/GL004i003p00125> doi: 10.1029/GL004i003p00125
- Kesich, A., Bonde, J., Egedal, J., Fox, W., Goodwin, R., Katz, N., & Le, A. (2008, JUN). Magnetic flux array for spontaneous magnetic reconnection experiments. *REVIEW OF SCIENTIFIC INSTRUMENTS*, 79(6). doi: 10.1063/1.2937193
- Le, A., Egedal, J., Ohia, O., Daughton, W., Karimabadi, H., & Lukin, V. S. (2013, MAR 28). Regimes of the Electron Diffusion Region in Magnetic Reconnection. , 110(13). doi: {10.1103/PhysRevLett.110.135004}
- Li, W.-Y., Khotyaintsev, Y. V., Tang, B.-B., Graham, D. B., Norgren, C., Vaivads, A., ... Wang, C. (2021). Upper-hybrid waves driven by meandering electrons around magnetic reconnection x line. *Geophysical Research Letters*, 48(16), e2021GL093164. Retrieved from <https://agupubs.onlinelibrary.wiley.com/doi/abs/10.1029/2021GL093164> (e2021GL093164 2021GL093164) doi: <https://doi.org/10.1029/2021GL093164>
- Papadopoulos, K. (1977). A review of anomalous resistivity for the ionosphere. *Reviews of Geophysics*, 15(1), 113-127. Retrieved from <https://agupubs.onlinelibrary.wiley.com/doi/abs/10.1029/RG015i001p00113> doi: 10.1029/RG015i001p00113
- Paschmann, G., & Daly, P. W. (1998, January). Analysis Methods for Multi-Spacecraft Data. ISSI Scientific Reports Series SR-001, ESA/ISSI, Vol. 1. ISBN 1608-280X, 1998. *ISSI Scientific Reports Series*, 1.
- Pritchett, P. (2001, MAR 1). Geospace environment modeling magnetic reconnection challenge: Simulations with a full particle electromagnetic code. , 106(A3), 3783-3798.
- Vasyliunas, V. M. (1975). Theoretical models of magnetic-field line merging .1. *Reviews of Geophysics*, 13(1), 303-336.
- Zhou, M., Deng, X. H., Zhong, Z. H., Pang, Y., Tang, R. X., El-Alaoui, M., ... Lindqvist, P.-A. (2019, jan). Observations of an electron diffusion region in symmetric reconnection with weak guide field. *The Astrophysical Journal*, 870(1), 34. Retrieved from <https://doi.org/10.3847/1538-4357/aaf16f> doi: 10.3847/1538-4357/aaf16f
- Zweibel, E. G., & Yamada, M. (2009). Magnetic reconnection in astrophysical and laboratory plasmas. *Annual Review of Astronomy and Astrophysics*, 47(1), 291-332. Retrieved from <https://doi.org/10.1146/annurev-astro-082708-101726> doi: 10.1146/annurev-astro-082708-101726